The identifying extended Kalman filter: parametric system identification of a vehicle handling model

M C Best*, **A P Newton,** and **S Tuplin**
Department of Aeronautical and Automotive Engineering, Loughborough University, Loughborough, UK

The manuscript was received on 17 March 2006 and was accepted after revision for publication on 9 May 2006.

DOI: 10.1243/14644193JMBD68

Abstract: This article considers a novel method for estimating parameters in a vehicle-handling dynamic model using a recursive filter. The well-known extended Kalman filter – which is widely used for real-time state estimation of vehicle dynamics – is used here in an unorthodox fashion; a model is prescribed for the sensors alone, and the state vector is replaced by a set of unknown model parameters. With the aid of two simple tuning parameters, the system self-regulates its estimates of parameter and sensor errors, and hence smoothly identifies optimal parameter choices.

The method makes one contentious assumption that vehicle lateral velocity (or body sideslip angle) is available as a measurement, along with the more conventionally available yaw velocity state. However, the article demonstrates that by using the new generation of combined GPS/inertial body motion measurement systems, a suitable lateral velocity signal is indeed measurable. The system identification is thus demonstrated in simulation, and also proved by successful parametrization of a model, using test vehicle data. The identifying extended Kalman filter has applications in model validation – for example, acting as a reference between vehicle behaviour and higher-order multi-body models – and it could also be operated in a real-time capacity to adapt parameters in model-based vehicle control applications.

Keywords: vehicle handling dynamics, Kalman filter, system identification, vehicle parameter

1 INTRODUCTION

Both on and off the vehicle, computing power continues to increase, making ever more complex models more practical for simulation experiments, vehicle design, and real-time applications such as chassis control. There is, however, still a significant role for simplified models, especially where a good correlation with measured vehicle behaviour is required. Complex multi-body models have the advantage of potential accuracy, but their vast parameter set often makes direct correlation with vehicle responses difficult – not because accurate sensor tracking is not possible, but rather in that multiple parameter combinations exist, which would achieve the same aim.

Conversely, the restricted parameter set of simpler models can be chosen to optimize the match with the vehicle, using a process of system identification. A suitable low-order model, with optimized parameter set can then be validated against both complex multi-body models and test vehicles, to provide a correlation process over a range of model orders. The reduced set of model parameters can also be adapted to the time-varying environment variables, vehicle inertia, tyre wear and pressure, and road friction.

Within the field of chassis control, the Kalman filter is now recognized as an effective tool for observing the dynamic states of a system – e.g. for vehicle ride [**1**] and handling control [**2**, **3**]. It also uses a simplified vehicle model, along with available sensor measurements, effectively supplementing the

Corresponding author: Department of Aeronautical and Automotive Engineering and Transport Studies, Loughborough University, Ashby Road, Loughborough LE11 3TU, UK. email: m.c.best@lboro.ac.uk

sensor information with predictions of state and sensor propagation from the model.

In this article, a new use for the extended, or non-linear, Kalman filter is explored, applying it in a modified form to perform the function of system identification rather than real-time estimation. The identifying extended Kalman filter (IEKF) operates in an unconventional way, in that its own internal model is restricted to prediction of the sensor set. The innovation sequence (modelled versus measured sensor errors) is then used to modify a 'state' vector that is defined as the subset of parameters to be identified. The basic premise is that, provided the available sensors are assumed to include the full state of the vehicle, the best model parameters can be derived from this – a standard assumption in the process of system identification, but novel in its execution by Kalman filter.

The method uses a bold and perhaps contentious assumption, however; by requiring the full state vector in the sensor set, it assumes knowledge of the traditionally hard to measure lateral velocity state. However, recent developments of combined differential GPS/inertial measurement systems make the assumption more reasonable, with commercially available (albeit expensive) systems currently declaring accuracies of 0.1 m/s in lateral velocity; in this article, one such system is used to prove that IEKF is practicable.

The IEKF design is first outlined in section 2. It is then examined in the simulation environment, with a two-degree-of-freedom non-linear handling model (section 3) identified from data generated on a more complex model in section 4. Finally, the method is proved using data measured from a test vehicle, in section 5.

2 IDENTIFYING EXTENDED KALMAN FILTER

The standard extended Kalman filter (EKF) operates on non-linear system and sensor models $\mathbf{f}$ and $\mathbf{h}$, which relate the true state vector $\bar{\boldsymbol{x}}$, measured sensor set $\boldsymbol{y}$, known inputs $\boldsymbol{u}$, and model parameters $\boldsymbol{\theta}$ at any instant k according to

$$\dot{\bar{\boldsymbol{x}}}_k = \mathbf{f}(\bar{\boldsymbol{x}}_k, \boldsymbol{u}_k, \boldsymbol{\theta}_k) + \boldsymbol{\omega}_k \tag{1}$$

$$\boldsymbol{y}_k = \mathbf{h}(\bar{\boldsymbol{x}}_k, \boldsymbol{u}_k, \boldsymbol{\theta}_k) + \boldsymbol{\upsilon}_k \tag{2}$$

(see for example reference [**4**]). $\boldsymbol{\omega}$ thus describes the state propagation modelling error, and $\boldsymbol{\upsilon}$ gives the sensor error. $\boldsymbol{\upsilon}$ is often misleadingly referred to as the measurement error, when in reality it aggregates measurement noise within $\boldsymbol{y}$, and sensor modelling errors in $\mathbf{h}$.

An optimal filter can be derived if the error sequences obey the following

$$E(\boldsymbol{\omega}_k) = \mathbf{0}, \quad E(\boldsymbol{\upsilon}_k) = \mathbf{0}, \ \forall k \tag{3}$$

$$E(\boldsymbol{\omega}_j \boldsymbol{\omega}_k^{\mathrm{T}}) = \mathbf{0}, \quad E(\boldsymbol{\upsilon}_j \boldsymbol{\upsilon}_k^{\mathrm{T}}) = \mathbf{0}, \ \forall (j \neq k) \tag{4}$$

$$\mathbf{Q}_k = E(\boldsymbol{\omega}_k \boldsymbol{\omega}_k^{\mathrm{T}}), \quad \mathbf{S}_k = E(\boldsymbol{\omega}_k \boldsymbol{\upsilon}_k^{\mathrm{T}}) = \mathbf{0},$$
$$\mathbf{R}_k = E(\boldsymbol{\upsilon}_k \boldsymbol{\upsilon}_k^{\mathrm{T}}) \tag{5}$$

where the error covariance matrices $\mathbf{Q}_k$, $\mathbf{R}_k$, and $\mathbf{S}_k$ are assumed known. In practice, they are difficult to estimate and their setting is a topic of continuing interest (see for example reference [**5**]). They are often assumed to be time-invariant, and are approximated, or even set nominally, with $\mathbf{S}$ often neglected as approximately zero. In this application, only initial conditions required for these matrices will be shown, with the true covariances being identified within the algorithm.

The EKF also requires model Jacobians to be evaluated at each time step, defined

$$\mathbf{F}(\hat{\boldsymbol{x}}_k) = \left.\frac{\partial \mathbf{f}(\boldsymbol{x}, \boldsymbol{u}_k, \boldsymbol{\theta}_k)}{\partial \boldsymbol{x}}\right|_{\boldsymbol{x}=\hat{\boldsymbol{x}}_k}$$
$$\mathbf{H}(\hat{\boldsymbol{x}}_k) = \left.\frac{\partial \mathbf{h}(\boldsymbol{x}, \boldsymbol{u}_k, \boldsymbol{\theta}_k)}{\partial \boldsymbol{x}}\right|_{\boldsymbol{x}=\hat{\boldsymbol{x}}_k} \tag{6}$$

and the full set of equations for the standard, real-time state estimation application are

$$\mathbf{F}_k^* = \mathbf{F}(\hat{\boldsymbol{x}}_k) - \mathbf{S}\mathbf{R}^{-1}\mathbf{H}(\hat{\boldsymbol{x}}_k) \tag{7}$$

$$\mathbf{K}_k = \mathbf{P}_k \mathbf{H}^{\mathrm{T}}(\hat{\boldsymbol{x}}_k)[\mathbf{H}(\hat{\boldsymbol{x}}_k)\mathbf{P}_k \mathbf{H}^{\mathrm{T}}(\hat{\boldsymbol{x}}_k) + \mathbf{R}]^{-1} \tag{8}$$

$$\mathbf{P}_k^* = [\mathbf{I} - \mathbf{K}_k \mathbf{H}(\hat{\boldsymbol{x}}_k)]\mathbf{P}_k \tag{9}$$

$$\mathbf{P}_{k+1} = \mathbf{P}_k^* + T[\mathbf{Q} - \mathbf{S}\mathbf{R}^{-1}\mathbf{S}^{\mathrm{T}} + \mathbf{F}^*(\hat{\boldsymbol{x}}_k)\mathbf{P}_k^* + \mathbf{P}_k^* \mathbf{F}^{*\mathrm{T}}(\hat{\boldsymbol{x}}_k)] \tag{10}$$

$$\hat{\boldsymbol{x}}_{k+1} = \hat{\boldsymbol{x}}_k + \mathbf{K}_k(\mathbf{y}_k - \mathbf{h}(\hat{\boldsymbol{x}}_k)) + T[\mathbf{f}(\hat{\boldsymbol{x}}_k) + \mathbf{S}\mathbf{R}^{-1}(\mathbf{y}_k - \mathbf{h}(\hat{\boldsymbol{x}}_k))] \tag{11}$$

where the filter sample time T is used to provide a simple Euler integration of the state derivatives.

Now the premise adopted in reference [**6**] is that an EKF can have its state vector augmented to include a subset of the model parameters. The resulting filter assumes no known model for the parameter variation, and simply ensures slow adaptation by adjusting the expectation of errors related to the parameter changes; so equation (1) becomes

$$\dot{\bar{\boldsymbol{z}}}_k = \begin{bmatrix} \dot{\bar{\boldsymbol{x}}}_k \\ \dot{\bar{\boldsymbol{\theta}}} \end{bmatrix} = \begin{bmatrix} \mathbf{f}(\boldsymbol{x}_k, \boldsymbol{u}_k, \boldsymbol{\theta}_k) \\ \mathbf{0} \end{bmatrix} + \begin{bmatrix} \boldsymbol{\omega}_k^{(x)} \\ \boldsymbol{\omega}_k^{(\theta)} \end{bmatrix} \tag{12}$$

and the covariance $E(\boldsymbol{\omega}_k^{(\theta)} \boldsymbol{\omega}_k^{(\theta)\mathrm{T}})$ is then set as a tuning parameter, to adjust the rate of adaptation, ensuring this is 'slow' compared with the state propagation dynamics.

The proposed identifying Kalman filter, IEKF takes this formulation one step further; provided the state vector is entirely represented as a subset of the sensor set, $\boldsymbol{x}_k \in \boldsymbol{y}_k$, the state vector can be formed entirely as a set of the parameters, such that equations (1) and (2) become

$$\dot{\boldsymbol{\theta}}_k = \boldsymbol{\omega}_k \tag{13}$$

$$\boldsymbol{y}_k = \mathbf{h}(\boldsymbol{y}_{k-1}, \boldsymbol{u}_{k-1}, \boldsymbol{\theta}_{k-1}) + \boldsymbol{\upsilon}_k \tag{14}$$

where the sensor equation is simply modified to include an Euler integrated propagation of each variable over a time step, to avoid identity equations. This reduces the system such that the entire model is represented within $\mathbf{h}$ alone. Note, however, that it also reduces the system to a form where the error covariance matrices can be determined from the noise sequences $\boldsymbol{\omega}_k$ and $\boldsymbol{\upsilon}_k$, as these are now directly calculable. The form of equations (1) and (2) depends on the unknown $\bar{\boldsymbol{x}}_k$, so the error covariances cannot be explicitly determined within that filter.

The IEKF propagates its own error covariances, so $\mathbf{Q}_k$, $\mathbf{R}_k$, and $\mathbf{S}_k$ are now time varying. Applying equations (13) and (14) to the EKF formulae of equations (7)–(11), and noting that now $\mathbf{f} = 0$ and $\mathbf{F} = 0$

$$\mathbf{H}(\hat{\boldsymbol{\theta}}_k) = \left.\frac{\partial \mathbf{h}(\boldsymbol{x}_k, \boldsymbol{u}_k, \boldsymbol{\theta})}{\partial \boldsymbol{\theta}}\right|_{\boldsymbol{\theta}=\hat{\boldsymbol{\theta}}_k} \tag{15}$$

$$\mathbf{K}_k = \mathbf{P}_k \mathbf{H}^{\mathrm{T}}(\hat{\boldsymbol{\theta}}_k)[\mathbf{H}(\hat{\boldsymbol{\theta}}_k)\mathbf{P}_k \mathbf{H}^{\mathrm{T}}(\hat{\boldsymbol{\theta}}_k) + \mathbf{R}_k]^{-1} \tag{16}$$

$$\mathbf{P}_k^* = [\mathbf{I} - \mathbf{K}_k \mathbf{H}(\hat{\boldsymbol{\theta}}_k)]\mathbf{P}_k \tag{17}$$

$$\begin{aligned}\mathbf{P}_{k+1} = {} & \mathbf{P}_k^* + T[\mathbf{Q}_k - \mathbf{S}_k \mathbf{R}_k^{-1} \mathbf{S}_k^{\mathrm{T}} \\ & - \mathbf{S}_k \mathbf{R}_k^{-1} \mathbf{H}(\hat{\boldsymbol{\theta}}_k)\mathbf{P}_k^* + \mathbf{P}_k^* \mathbf{H}(\hat{\boldsymbol{\theta}}_k)\mathbf{R}_k^{-1} \mathbf{S}_k^{\mathrm{T}}]\end{aligned} \tag{18}$$

$$\begin{aligned}\hat{\boldsymbol{\theta}}_{k+1} = {} & \hat{\boldsymbol{\theta}}_k + (\mathbf{K}_k + T\mathbf{S}_k \mathbf{R}_k^{-1}) \\ & \times (\boldsymbol{y}_k - \mathbf{h}(\boldsymbol{y}_k, \boldsymbol{u}_k, \hat{\boldsymbol{\theta}}_k))\end{aligned} \tag{19}$$

where

$$\mathbf{Q}_{k+1} = (1-\alpha)\mathbf{Q}_k + \alpha\lambda^2 \boldsymbol{\omega}_k \boldsymbol{\omega}_k^{\mathrm{T}} \tag{20}$$

$$\mathbf{S}_{k+1} = (1-\alpha)\mathbf{S}_k + \alpha\lambda \boldsymbol{\omega}_k \boldsymbol{\upsilon}_k^{\mathrm{T}} \tag{21}$$

$$\mathbf{R}_{k+1} = (1-\alpha)\mathbf{R}_k + \alpha \boldsymbol{\upsilon}_k \boldsymbol{\upsilon}_k^{\mathrm{T}} \tag{22}$$

with

$$\boldsymbol{\omega}_k = \frac{1}{T}(\hat{\boldsymbol{\theta}}_{k+1} - \hat{\boldsymbol{\theta}}_k) \tag{23}$$

$$\boldsymbol{\upsilon}_k = \boldsymbol{y}_{k+1} - \mathbf{h}(\boldsymbol{y}_k, \boldsymbol{u}_k, \hat{\boldsymbol{\theta}}_k) \tag{24}$$

Apart from suitable nominal initial conditions for $\mathbf{Q}_0$, $\mathbf{R}_0$, and $\mathbf{S}_0$, two tuning parameters are now required, α and λ. α applies an exponentially weighted moving average to the propagation of the noise matrices in order to introduce an appropriate memory of the error history into the covariance. It can better be interpreted in terms of the filtering time constant, τ it introduces, using

$$\alpha = 1 - e^{(T/\tau)} \tag{25}$$

λ performs a similar function to the design covariance $E(\boldsymbol{\omega}_k^{(\boldsymbol{\theta})} \boldsymbol{\omega}_k^{(\boldsymbol{\theta})\mathrm{T}})$ in reference [**6**]. Set in the range $0 < \lambda < 1$, it diminishes the expectation of error in the change in parameters, stabilising the identification. The filter causes parameter adaptation, which induces (a desirable) non-zero $\dot{\boldsymbol{\theta}}_k$. However, these changes are *errors* according to the zero model of equation (13), and if their *total* magnitude is interpreted as error, $\mathbf{Q}_k$ becomes relatively large compared with $\mathbf{R}_k$, which results in an increase in the feedback gain $\mathbf{K}_k$ to provide greater correction to the $\boldsymbol{\theta}$. Subsequent parameter corrections are then larger, and this induces instability. λ provides a means of balancing the filter such that the changes in $\mathbf{Q}_k$ are, correctly, not interpreted entirely as error.

3 IDENTIFIED AND SOURCE MODELS

A means of testing the method within a known environment is sought to explore variations of tuning parameters and define measures of success. A non-linear identification model is clearly required, so the simple 'bicycle' model (see for example, reference [**7**]), with Pacejka tyre non-linearity (see reference [**8**]) is used

$$\dot{v} = \frac{(\mathbf{F}_{yf} + \mathbf{F}_{yr})}{mM_0 - ur} \tag{26}$$

$$\dot{r} = \frac{(a\mathbf{F}_{yf} - (L-a)\mathbf{F}_{yr})}{iI_{ZZ0}} \tag{27}$$

with front and rear tyre forces aggregated over the two tyres at each axle

$$\begin{aligned}\mathbf{F}_{yf/r} = {} & p_{f/r}\mathbf{F}_0 \sin[c_{f/r} \tan^{-1} \\ & \{\bar{\alpha}_{f/r} - e_{f/r}(\bar{\alpha}_{f/r} - \tan^{-1}(\bar{\alpha}_{f/r}))\}]\end{aligned} \tag{28}$$

based on normalized slip angles

$$\bar{\alpha}_{f/r} = \frac{g_{f/r} C_{\alpha 0} \alpha_{f/r}}{c_{f/r} p_{f/r} \mathbf{F}_0} \tag{29}$$

where f/r refers to front/rear axles appropriately, and the slip angles are given by

$$\alpha_f = \frac{(-v - ar)}{u + \delta}, \quad \alpha_r = \frac{(-v + (L-a)r)}{u} \tag{30}$$

Table 1 lists default values for the model parameters, which are set to emulate an E class, large executive saloon (from an Appendix of reference [**9**]), and thus provide a test comparable with the vehicle identification as shown, in section 5. The inertia values are specified as multiples of two parameters in order to normalize the variables that might be identified. In section 4, $\boldsymbol{\theta}$ is chosen as a subset of $[a, m, i, p_f, g_f, c_f, e_f, p_r, g_r, c_r, e_r]$ with the remaining parameters set to default values. As the Kalman filter objective is minimization of trace($\mathbf{P}$), selection of parameters of equal order allows approximately equal priority to be placed on each identified parameter.

From equations (26) and (27) the required definition of the IEKF model of equation (14) is

$$\boldsymbol{y} = \begin{bmatrix} v \\ r \end{bmatrix},$$

$$\mathbf{h}_k = \begin{bmatrix} v_{k-1} + \left. \dfrac{T\{(\mathbf{F}_{yf} + \mathbf{F}_{yr})}{mM_0 - ur\}} \right|_k \\ r_{k-1} + \left. \dfrac{T(a\mathbf{F}_{yf} - (L-a)\mathbf{F}_{yr})}{iI_{ZZ0}} \right|_k \end{bmatrix} \tag{31}$$

and for implementation, the $\mathbf{H}$ Jacobian is formed using the analytical Math toolbox (Symbolic Maths in Matlab), with the resulting expression copied into the Kalman filter code.

The source data are generated using a higher-order model [**10**], incorporating roll and longitudinal dynamics, and four load-dependent friction circle limited tyres with appropriate relaxation lags; the precise model equations and parameter set are provided in the Appendix 2. Note that the detail of this model and, even to some extent, the accuracy of the source data are themselves of secondary importance; the study should reveal similar results for any suitably formulated high-order model. It is the extent to which the identified parameters can approximate the source model within the context of the simpler identification model, which is key here.

Table 1 Identification model parameters emulating an executive saloon

	Parameter	Value (default)	Units
Wheelbase	L	3.1	m
Normalizing mass	M_0	2000	kg
Normalizing yaw moment of inertia	I_{ZZ0}	4800	kg m^2
Normalizing peak lateral tyre force (2 tyres)	$\mathbf{F}_0$	9320	N
Normalizing cornering stiffness (2 tyres)	$C_{\alpha 0}$	227	kN/rad
CG to front axle distance	a	1.3	m
Mass multiplier	m	0.9	–
Yaw inertia multiplier	i	0.9	–
Peak tyre force multiplier	p_f, p_r	1, 1	–
Tyre force gain (cornering stiffness) multiplier	g_f, g_r	1, 1	–
Tyre model shape parameter (Pacejka, C)	c_f, c_r	1.4, 1.4	–
Tyre model shape parameter (Pacejka, E)	e_f, e_r	−0.2, −0.2	–

4 SIMULATION EXPERIMENT

In this section, the aims are to explore the operation and tuning of IEKF and conduct a full identification to test the method. First, note from equations (26) – (30) that the full parameter set cannot be optimized together; the system is over-determined, and the optimization would be confounded by combinations of g, m, and i. Therefore a two-stage process is conducted, starting with a low-amplitude test to establish the 'inertia' parameter set

$$\boldsymbol{\theta} = \begin{bmatrix} m & i & a \end{bmatrix}^{\mathrm{T}}$$

within the linear region of the tyres; the remaining parameters are set at their $\boldsymbol{\theta}_0$ values in Table 1.

Source model test data are generated on a random steer input at fixed speed $u = 25$ m/s. (Constant forward speed is maintained by a simple proportional feedback control on the applied engine torque in the source model.) The input is 60 s of Gaussian white noise with a sampling period $T = 0.01$ – also used for the IEKF. This is filtered in the frequency domain to remove all frequencies >5 Hz in order to restrict the input frequencies to those which a human driver could be expected to achieve in a real vehicle. The signal amplitude is then scaled to give an RMS steer angle $\delta_{\mathrm{RMS}} = 0.57^\circ$, in order to achieve peak lateral accelerations of around 4 m/s^2.

The source data are applied to the IEKF, with no additional measurement noise – the significant differences between source and identified model structure comprise the only error sources at this stage. Four cases are considered, to explore the importance of particular choices of τ, λ, and $\boldsymbol{\theta}_0$; these are listed in Table 2. In all cases, the parameter error covariance matrices have been initialized nominally, as $\mathbf{Q}_0 = 10^{-4}\,\mathbf{I}$, $\mathbf{S}_0 = 0$. $\mathbf{R}_0$ is then set by

Table 2 IEKF parameter and initialization settings

Case	m_0	i_0	a_0	τ	λ
1	0.45	0.45	0.65	60	0.01
2	0.9	0.9	1.3	60	0.01
3	0.9	0.9	1.3	600	0.01
4	0.9	0.9	1.3	60	0.1

calculating a time history for v_k from equation (24), using the source and initial identification model, and setting $\mathbf{R}_0 = \text{cov}(v_k)$.

Given the recursive configuration of the IEKF, to establish an averaged result, the source data are repeatedly passed through the filter with the free variables allowed to vary continuously throughout. Figure 1 shows the results over 30 iterations to illustrate convergence. Plots (a)–(c) show the parameter variation, and (d)–(f) illustrate the variations of selected, but typical components within the error matrices. It should be noted that values in **P** and **Q** reflect the filter's estimate of error, whereas $\mathbf{R}_k$ provides a more verifiable measure of performance – the filter versus source error in the measurements (the innovations). Trace(**R**) shows the aggregated performance over the two sensors.

As an independent measure of performance, the converged parameter sets are applied in an open-loop validation of the identification model, with u_k and δ_k provided from the source model, over a separate but similar band limited white noise test. Results are summarized in Table 3.

The results are good, with an average 72 per cent reduction in $\hat{v}$ error and 48 per cent reduction in $\hat{r}$ error in the successful cases 1–3. The identified parameters are close to the anticipated values; a perfect match of course is not expected, as the identified values achieve a better match to the data, compensating the differences between the model structures. Trace(**R**) and plots (a)–(c) also show that convergence is possible within just 10–15 iterations.

There is a small difference between the parameters identified by cases 1 and 2, which differ only in their starting points, $\boldsymbol{\theta}_0$. This is because the IEKF operates on the local gradient function $\mathbf{H}_k$, and the sensor error is adapting multiple parameters to minimize the scalar, trace(**P**). The method will therefore find the local minimum from a given starting point, and uniqueness will also depend on the conditioning of the parameter space. Tuning of the IEKF does not alter the converged results, but the performance difference is reasonably small and remains small for other starting points that were tried.

$\tau = 60$ has been set nominally to match the test duration, and case 3 considers an alternative, higher setting. The effect is two-fold; the parameter convergence is slowed because τ directly slows adaptation of the error covariance matrices (plots (d)–(f)). This maintains **Q** at higher values for longer, causing more parameter variation within each iteration, because greater expectation of parameter ('process') error increases the sensor error feedback by increasing the Kalman gain **K**. The converged parameters in Table 3 are very similar to case 2, however, (note that i continues to increase beyond iteration 30 – not shown) and provided τ is not 'small', it can be set nominally. Similarly, the initial setting of $\mathbf{Q}_0$ can be set nominally, and/or adjusted to control the higher-frequency parameter variations.

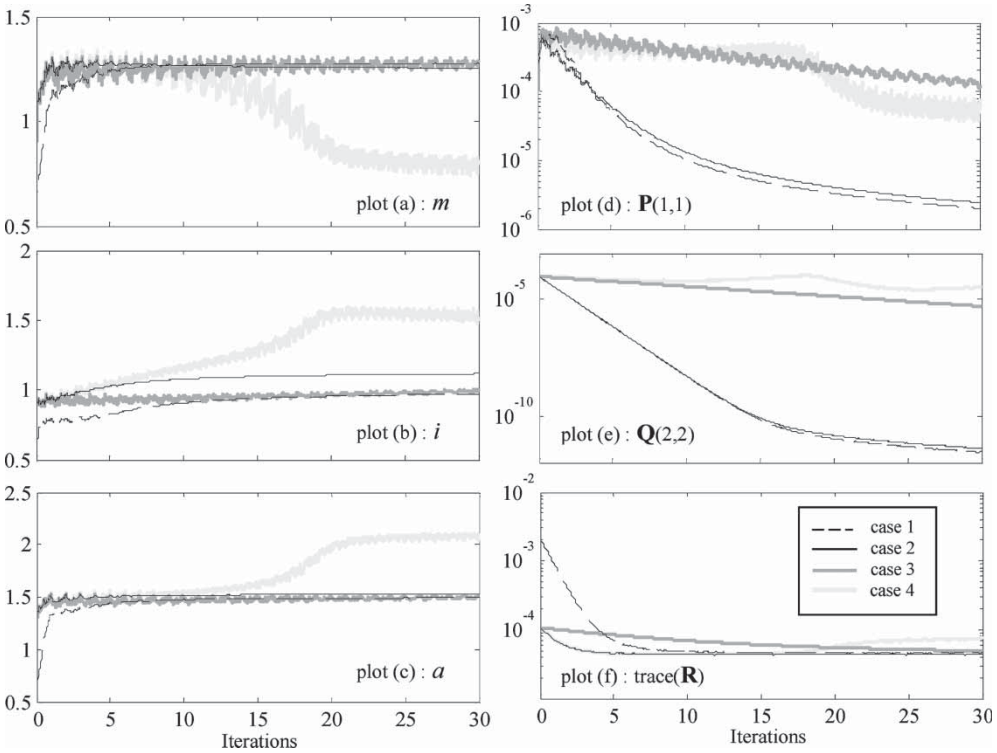

Fig. 1 Parameter and error covariance convergence

Table 3 Identified inertia model and performance

Error variance ($\times 10^{-3}$)	Reference ($\boldsymbol{\theta}_0$)	Case 1	Case 2	Case 3	Case 4
$\hat{v}$	9.02	2.89	2.36	2.33	2.18
$\hat{r}$	0.272	0.146	0.136	0.141	0.899
Identified parameters					
m	(0.90)	1.28	1.25	1.25	0.80
i	(0.90)	0.97	1.12	1.13	1.50
a	(1.30)	1.49	1.53	1.54	2.06

Selection of λ is more critical, as this governs the (fixed) proportion of parameter changes, which is interpreted as error. Higher settings of λ have a similar effect on $\mathbf{Q}$ as high τ or $\mathbf{Q}_0$, but here this can lead to instability as $\mathbf{R}$ reduces. The effect is illustrated by case 4, where $\lambda = 0.1$ is very close to the limit of stability. The parameters still converge, but the time histories of $\mathbf{P}$, $\mathbf{Q}$, and $\mathbf{R}$ all show the result to be invalid. As with τ, λ does not need to be finely tuned, provided a suitably low setting is made.

The identification is completed by now fixing the inertia parameters (from case 2) and optimizing the four Pacejka tyre parameters governing lateral force at each axle

$$\boldsymbol{\theta} = \begin{bmatrix} p_\mathrm{f} & g_\mathrm{f} & c_\mathrm{f} & e_\mathrm{f} & p_\mathrm{r} & g_\mathrm{r} & c_\mathrm{r} & e_\mathrm{r} \end{bmatrix}^\mathrm{T}$$

To excite the full range of force and slip, the same white noise process is employed, but now it is scaled up to $\delta_{\mathrm{RMS}} = 2.3^\circ$ to induce peak lateral accelerations of 8 m/s^2.

With τ, λ, and $\mathbf{Q}_0$, $\mathbf{R}_0$, $\mathbf{S}_0$ set as for cases 1 and 2, the IEKF results are given in Fig. 2. A higher number of iterations is now required, because of the increased order of the parameter space and the inter-dependence of the variables, but the process is not computationally expensive – 50 iterations take <3 min on the mid-range PC running Matlab used here. Table 4 lists the final identified model parameters and again the performance on independent validation data is considered; Fig. 3 shows the initial and final model response over a typical section of this data.

It is interesting that both reference and the identified tyre models over-estimate the tyre forces, when compared with the source model tyre data (Fig. 2(e) and (f)). The reference model error is largely due to neglecting load transfers that reduce the total

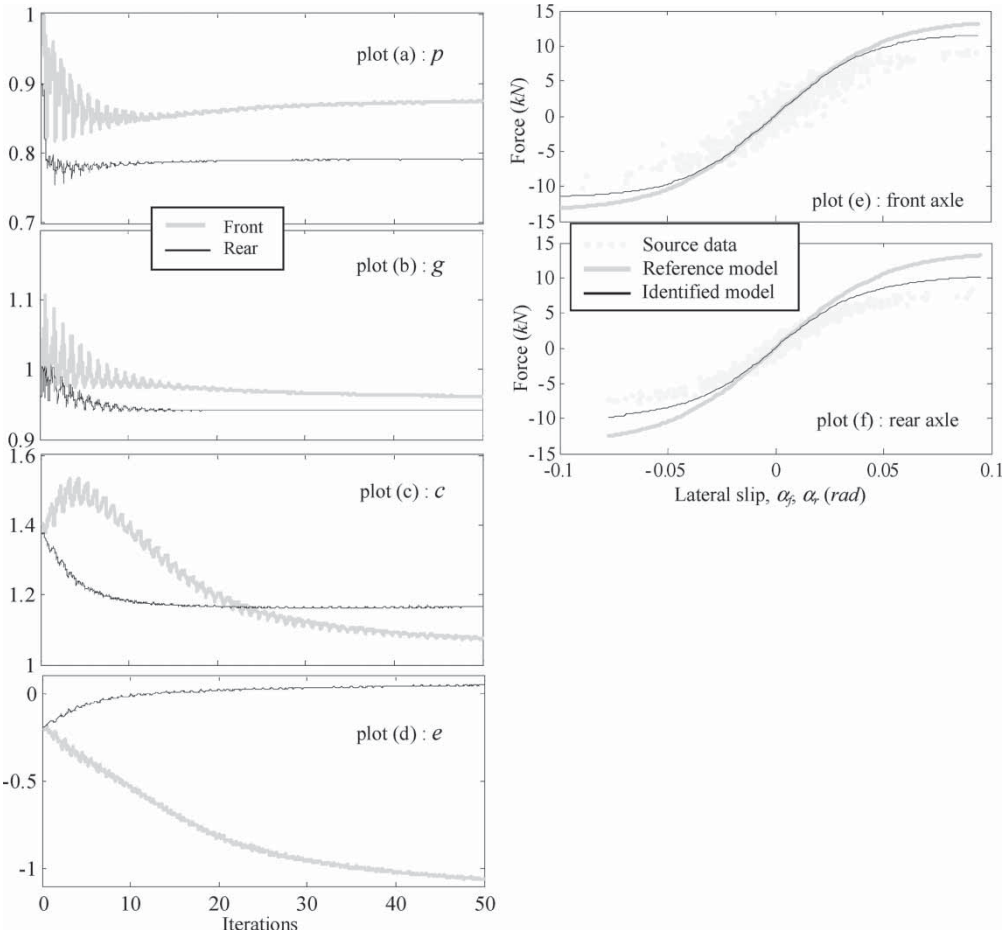

Fig. 2 Tyre parameter convergence

Table 4 Validation of identified model (simulated)

Error variance ($\times 10^{-3}$)	Reference ($\boldsymbol{\theta}_0$)	IEKF
$\hat{v}$	78.3	28.0
$\hat{r}$	4.89	1.01
Identified parameters		
m	0.9	1.25
i	0.9	1.12
a	1.3	1.53
p_f, p_r	1.0, 1.0	0.87, 0.79
g_f, g_r	1.0, 1.0	0.96, 0.94
c_f, c_r	1.4, 1.4	1.08, 1.17
e_f, e_r	−0.2, −0.2	−1.05, 0.05

tyre force in the source model (and in reality); the identified model generates lower forces (see p and g values in Table 4), but still seems to over-estimate. The model is consistent, however, as it operates with a mass estimation 25 per cent higher than the source model ($\hat{m} = 1.25$). Hence, both achieve similar lateral accelerations, and the states are accurately tracked as seen in Table 4 and Fig. 3. Of course, the tyre and inertia parameters are inter-dependent, so the inertia values would be lower if g had been set at a lower default value in the identification of $\boldsymbol{\theta} = \begin{bmatrix} m & i & a \end{bmatrix}^{\mathrm{T}}$. In reality, tyre and inertia values would not be simultaneously unknown, or (more practically) the parameters could separately be determined using other vehicle modes – e.g. ride or powertrain dynamics to determine mass, and longitudinal/lateral motion to determine tyres.

5 TEST VEHICLE EXPERIMENT

In order to prove that it is possible to use measured lateral velocity to good effect within the IEKF, and that the filter is a practicable concept, it is now applied to data recorded from an instrumented test vehicle; a Jaguar XJ8 saloon equipped with an RT3200 GPS/inertial measurement system was used. The vehicle CAN steering wheel measurement was synchronized with u, v, r, and a_y signals from the RT3200 and recorded at 100 Hz.

Test drives were conducted on a flat proving ground circuit in wet weather with some patches of standing water. Three test scenarios were considered:

(a) constant speed ($u = 15$ m/s), random steer;
(b) constant speed ($u = 20$ m/s) track circuits comprising a range of steady-state cornering with some additional step-steer events superimposed;
(c) track circuits as (b) but with additional acceleration and braking events included in combination with steering.

Interestingly, the IEKF did not prove to be effective on the random-steer test. The parameters converged, but the identification model performance was disappointing, with large phase errors blighting the lateral velocity estimate. Subsequent tests show that the IEKF/identification model combination is capable of good performance, so the conclusion at this stage is that the measurement of v is not sufficiently accurate in this type of test – the absence of steady-state cornering is a likely cause.

The identification is thus carried out on test (b), with test (c) used as a validation sequence. Also, as the wet track conditions limited peak lateral acceleration, both inertia and tyre identification are conducted on the same test. A total of 150 s of data was recorded for test (b) and the IEKF result for

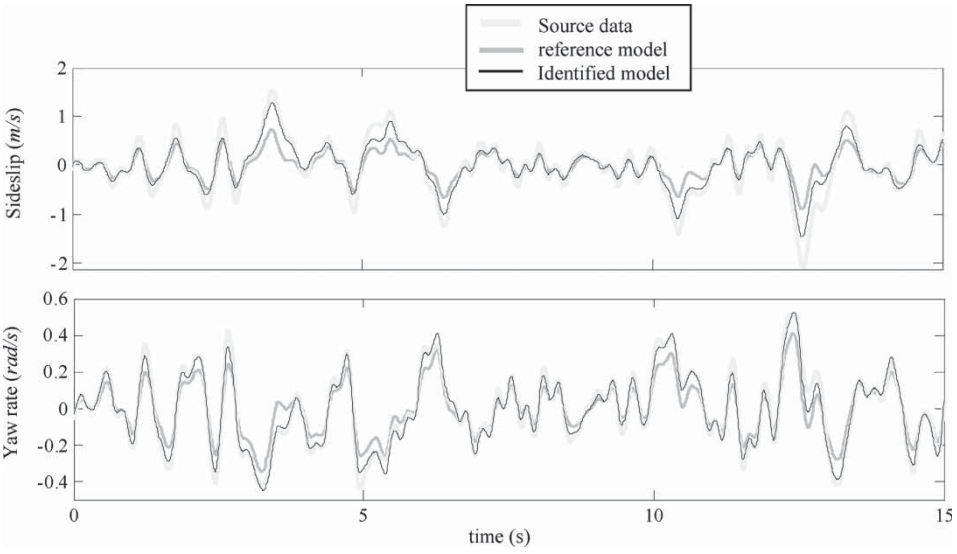

Fig. 3 Simulation experiment validation

$\tau = 100$, $\lambda = 0.01$, $\mathbf{Q}_0 = 10^{-4}\mathbf{I}$, $\mathbf{S}_0 = 0$ is summarized in Fig. 4.

As previously, these results were achieved in two stages, with inertia parameters (plots (a) and (b)) conducted first and then m, i, and a fixed for the tyre identification process (plots (c)–(f)). The parameter convergence is good, taking just 15 iterations, and note that the tyre shape parameters, c and e converge more slowly than the peak and cornering coefficient variables p and g. c and e act in combination to adjust the shape of the tyre model – particularly at higher slip angles, and these are less critical in establishing the basic force / slip relationship. **P** and **Q** are not plotted, as these behave in a very similar way to that seen in the simulation experiment.

The only unexpected result is $g \sim 0.5$. Early results for m and i showed inertia figures between 2 and 2.5 – values which are known to be incorrect. However, these were based on the setting $g = 1$, and as the default tyre model is entirely nominal and the road conditions wet, the inertia values were reoptimized with $g = 0.5$. Of course, this decision then causes g to be identified very close to 0.5 in the subsequent tyre identification on the same data; whereas the setting of g can be criticized as arbitrary, and the resulting inertia parameters as inconclusive, the results still represent an optimal combination.

The identified model is summarized in Table 5, and its performance is compared with the reference model (also having $g = 0.5$) on the identification source data and the independent validation data. The relationship between identified and reference parameters is similar to that seen in the simulation study, with the expected similarity in order of magnitudes (except in c and e for the reasons discussed earlier). Further, the convergence of $p_f = 0.74$, $p_r = 0.78$ is very encouraging, as p is essentially the model friction coefficient, and these values correspond very well to expectations of a wet road surface.

Time histories for these results are shown in Figs 5 and 6, respectively. The performance is excellent, with near-perfect tracking of r and also a_y – recall that the IEKF does not include a_y as a sensor. The reference result is quite poor, largely because the peak forces (p) are assumed higher, which results in exaggerated peaks in all of v, r, and a_y. The comparison might

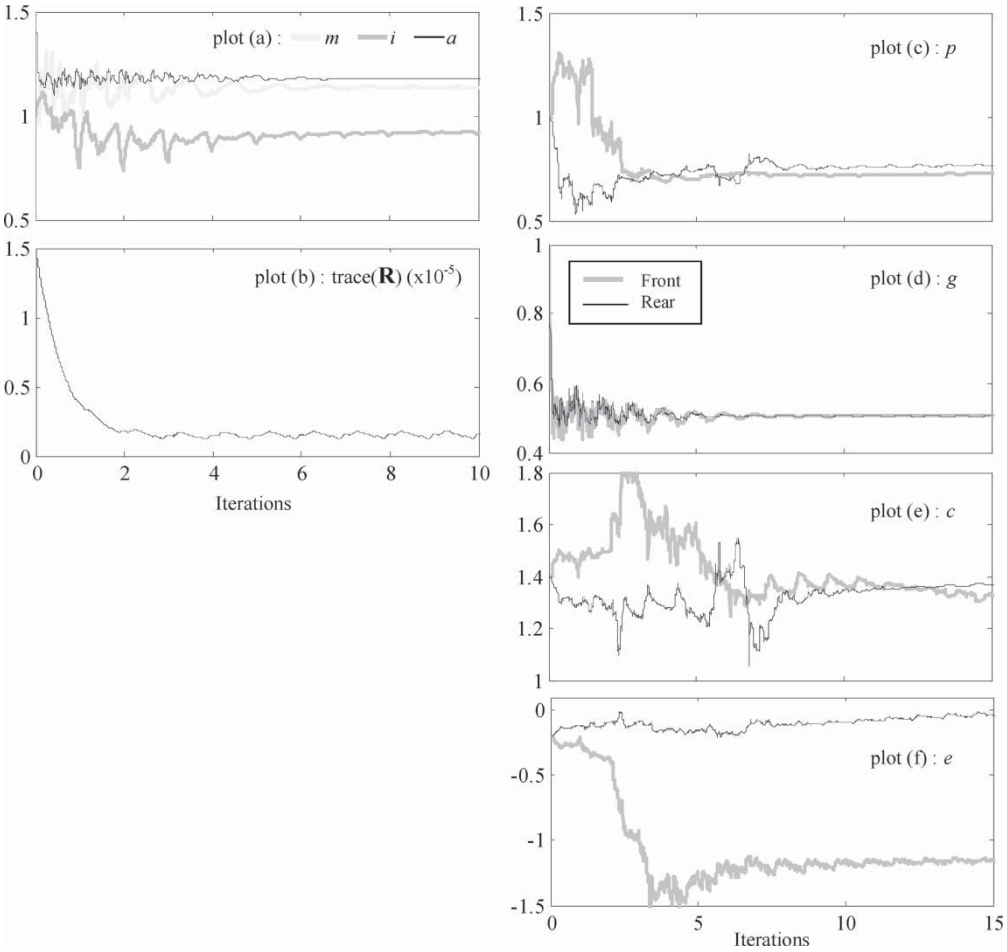

Fig. 4 Vehicle identification; parameter and error covariance convergence

Table 5 Validation of identified model (test vehicle)

Error variance ($\times 10^{-3}$)	Reference ($\boldsymbol{\theta}_0$)	IEKF
Source data test (b)		
$\hat{v}$	36.8	3.94
$\hat{r}$	3.03	0.05
Validation data test (c)		
$\hat{v}$	292.6	24.6
$\hat{r}$	11.6	0.57
Identified parameters		
m	1.0	1.14
i	1.0	0.93
a	1.5	1.18
p_f, p_r	1.0, 1.0	0.74, 0.78
g_f, g_r	0.5, 0.5	0.51, 0.50
c_f, c_r	1.4, 1.4	1.23, 1.43
e_f, e_r	−0.2, −0.2	−1.15, 0.04

seem to flatter the identified model (the reference could be improved by a simple reduction in the road surface friction coefficient), but it should be borne in mind that both identified and reference time histories are open-loop simulations, using only the measured steer input and vehicle speed.

The traces of v are particularly encouraging, as the sceptical vehicle dynamicist may not expect a good enough lateral velocity measurement for this application. Looking at Fig. 5, it can be seen that higher frequency variations are not tracked reliably in v, but that the gross variations are – and note the very low lateral velocities that are generated here. The noise-to-signal ratio in v is very high (87 per cent RMS error to RMS signal after optimization); yet the IEKF remains stable and returns parameters that yield a 10-fold improvement in estimation of v.

The validation data show greater lateral accelerations and velocities, due in part to the combined longitudinal acceleration, so the challenge for the model is greater, yet the performance is similarly impressive.

6 CONCLUDING REMARKS

The results show the IEKF to be a versatile, stable, and an easily configured process for system identification. The technique has been shown to be effective, both within the simulated environment – and hence for model-order reduction applications – and in identification from test vehicle data. Moreover, the very high levels of error between modelled and measured lateral velocity did not present an obstacle to success.

The method addresses three factors, which other more common system identification processes lack.

1. Any subset of parameters can be identified within a general non-linear form of model. The only restrictions are that the model must be smoothly non-linear, and the parameters must be suitably independent of each other.
2. The filter self-regulates and depends on just two tuning parameters, both of which can be set nominally within generous bounds.

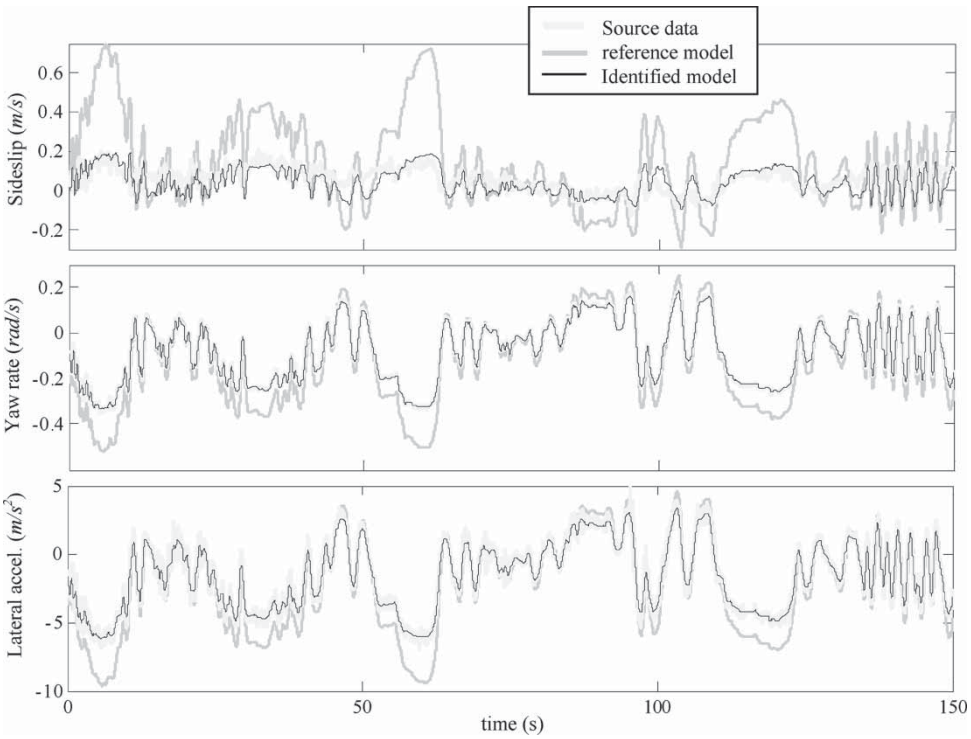

Fig. 5 Vehicle identification; fit to source data

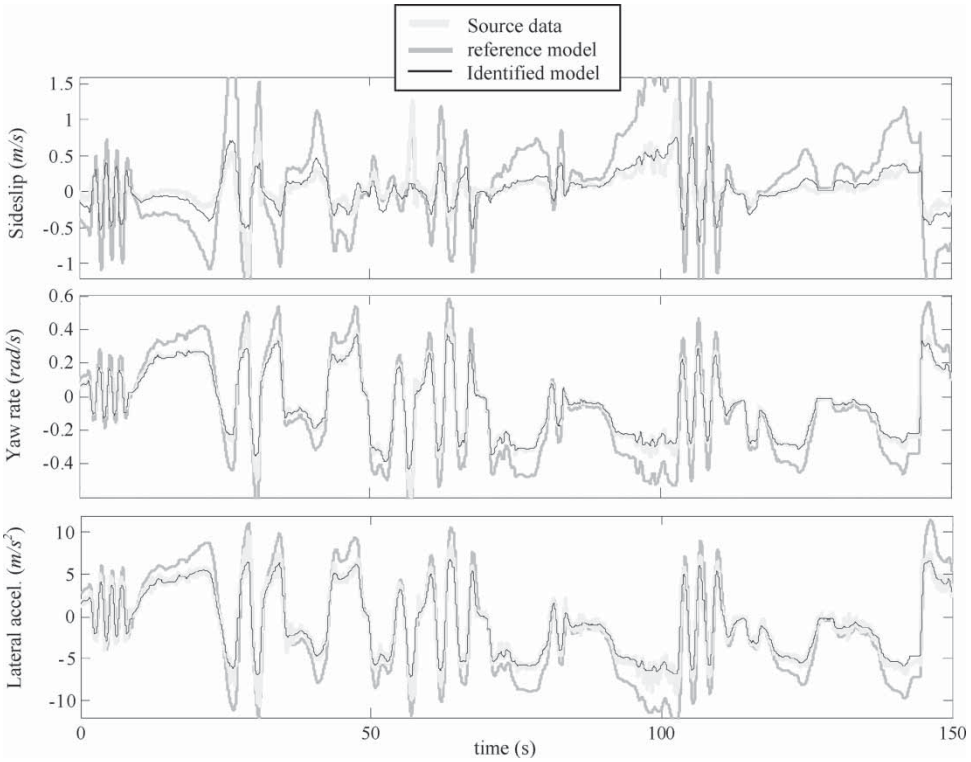

Fig. 6 Vehicle identification; fit to validation data

3. By varying the filter time constant, it can be set to operate over a long or short time-frame. Thus, it can be employed for off-line identification from a data set, or for on-line parameter adaptation to compensate changes in the vehicle environment.

The next steps for development are to conduct further vehicle-based experiments and to explore slightly higher-order identification model structures, particularly with a view to providing ride and drivetrain parameters, along with combined lateral/longitudinal tyre force models. Given the success of this first experiment, IEKF should become a valuable tool for all applications of reduced-order models.

REFERENCES

1 **Best, M. C.** and **Gordon, T. J.** A factorial analysis of Kalman filtering for semi-active vehicle suspension control. Proceedings from the ESDA/ASME European Joint Conference on *Engineering systems design and analysis*, London, UK, July 1994.

2 **Wenzel, T. A., Burnham, K. J., Blundell, M. V.,** and **Williams, R. A.** Dual extended Kalman filter for vehicle state and parameter estimation. *Veh. Syst. Dyn.*, 2006, **44**(2), 153–171.

3 **Arndt, C., Karidas, J.,** and **Busch, R.** Estimating non-measured vehicle States with an extended linearised Kalman filter. *Rev. Autom. Eng.*, 2005, **26**(1), 91–98.

4 **Gelb, A.** (Ed.). *Applied optimal estimation*, 1974 (MIT Press, Cambridge, MA, USA).

5 **Haykin, S.** (Ed.). *Kalman filtering and neural networks*, 2001 (John Wiley, New York).

6 **Best, M. C., Gordon, T. J.,** and **Dixon, P. J.** An extended adaptive Kalman filter for real-time State estimation of vehicle handling dynamics. *Veh. Syst. Dyn.*, 2000, **34**(1), 57–75.

7 **Gillespie, T. D.** *Fundamentals of vehicle dynamics*, 1992, pp. 195–207 (SAE Int., Warendale, PA, US).

8 **Milliken, D. L.** and **Milliken, W. F.** *Race car vehicle dynamics*, 1995, pp. 473–480 (SAE Int., Warrendale, PA, US).

9 **Dixon, J. C.** *Tires, suspension and handling*, 1996 (Arnold, London).

10 **Gordon, T. J.** and **Best, M. C.** On the synthesis of driver inputs for the simulation of closed-loop handling manoeuvres. *Int. J. Veh. Des.*, 2006, **40**(1–3), 52–76.

11 **Pacejka, H. B.** *Tyre and vehicle dynamics*, 2002 (Butterworth Heinemann, Oxford, UK and Woburn Massachusetts, US).

APPENDIX 1

Notation

a_y	CG lateral acceleration (m/s^2)
f	non-linear system model
F	system model Jacobian
h	non-linear sensors model
H	sensors model Jacobian

K	optimal gain matrix
P	state error covariance matrix
Q	process error covariance matrix
r	yaw rate (rad/s)
R	sensors error covariance matrix
S	sensors/process error cross covariance matrix
T	filter sampling interval(s)
u	forward velocity (m/s)
$\boldsymbol{u}$	vector of inputs
v	sideslip velocity (m/s)
$\boldsymbol{x}$	state vector
$\boldsymbol{y}$	sensors vector
α	moving average constant (see τ)
τ	moving average time constant for noise matrix 'memory'
δ	(front) wheel steer angle (rad)
$\boldsymbol{\theta}$	parameters vector
λ	parameter error scaling factor
$\boldsymbol{\upsilon}$	sensors error
$\boldsymbol{\omega}$	process (model) error
$\wedge$	caret denotes estimated value

Subscripts

k,f,r	subscripts denote time step, front, and rear, respectively

Superscripts

(x), (θ)	superscripts, relating to state or parameter errors, respectively

APPENDIX 2

Source model dynamics

The source model is based on the well-known three-degree-of-freedom model, simulating yaw, roll, and sideslip using a load-dependent, combined-slip Pacejka tyre model. A fourth, longitudinal degree-of-freedom is also included, as are additional dynamics for wheel-spin, and first-order lags for tyre relaxation. The principal model notation and parameter values are given in Table 6.

The equations of motion are longitudinal

$$M\dot{u} = \sum_{i=1,4} \mathbf{F}_{xi} + Mrv + Mhrp \tag{32}$$

lateral

$$M\dot{v} + Mh\dot{p} = \sum_{i=1,4} \mathbf{F}_{yi} - Mur \tag{33}$$

Table 6 Source vehicle model notation and parameter values

States and dynamic variables (units)	
u	vehicle forward velocity (m/s)
v	sideslip velocity (m/s)
p	roll angular velocity (rad/s)
r	yaw angular velocity (rad/s)
ϕ	roll angle (rad)
T_i	driveline or brake torque at wheel i
ω	wheel angular velocity (rad/s)
w	magnitude of tyre vertical load (N)
Parameters (value, units)	
I_{xx}	body roll moment of inertia (500 kg m^2)
I_{zz}	yaw moment of inertia (4800 kg m^2)
I_{xz}	roll/yaw product of inertia (0 kg m^2)
I_w	wheel (plus associated driveline) moment of inertia (5 kg m^2)
M	vehicle mass (2000 kg)
a	longitudinal distance of C of G to front axle (1.5 m)
b	longitudinal distance of C of G to rear axle (1.6 m)
h	C of G height above roll axis (0.45 m)
h_0	ground plane to roll axis distance below C of G (0.22 m)
h_f	front suspension roll centre height above ground (0.06 m)
h_r	rear suspension roll centre height above ground (0.4 m)
t_f	front track (1.55 m)
t_r	rear track (1.55 m)
r_r	tyre rolling radius (0.3 m)
K_f	front roll stiffness (27.8 kNm/rad)
K_r	rear roll stiffness (20.4 kNm/rad)
B_f	front roll damping (1800 Nms/rad)
B_r	rear roll damping (1800 Nms/rad)
B, C, D, E	Pacejka formula coefficients (1.0, 1.4, 1.0, −0.2 – dimensionless)
c_1, c_2	cornering stiffness parameters (69 kN/rad, 1.4 kN)
τ	time-constant for tyre relaxation (0.025 s)

yaw

$$I_{zz}\dot{r} + (\varepsilon I_{zz} - I_{xz})\dot{p} = a\sum_{i=1,2} \mathbf{F}_{yi} - b\sum_{i=3,4} \mathbf{F}_{yi} \tag{34}$$

roll

$$\begin{aligned} &-I_{xz}\dot{r} + Mh\dot{v} + (I_{xx} - \varepsilon I_{xz})\dot{p} \\ &\quad = -Mhur - (B_\mathrm{f} + B_\mathrm{r})p + (Mgh - K_\mathrm{f} - K_\mathrm{r})\phi \\ &\quad + (h_\mathrm{f} - h_0)\sum_{i=1,2} \mathbf{F}_{yi} + (h_\mathrm{r} - h_0)\sum_{i=3,4} \mathbf{F}_{yi} \end{aligned} \tag{35}$$

roll kinematics

$$\dot{\phi} = p \tag{36}$$

Standard SAE axes are used [**7**] fixed relative to the vehicle wheelbase; the wheels are labelled (1–4) in ascending order as front-left, front-right, rear-left, rear-right.

The forces ($\mathbf{F}_{xi}$, $\mathbf{F}_{yi}$) controlling the vehicle motion allow for large steer angles

$$\begin{aligned} \mathbf{F}_{x1,2} &= \mathbf{F}^*_{tx1,2}\cos\delta - \mathbf{F}^*_{ty1,2}\sin\delta, \quad \mathbf{F}_{x3,4} = \mathbf{F}^*_{tx3,4} \\ \mathbf{F}_{y1,2} &= \mathbf{F}^*_{ty1,2}\cos\delta - \mathbf{F}^*_{tx1,2}\sin\delta, \quad \mathbf{F}_{y3,4} = \mathbf{F}^*_{ty3,4} \end{aligned} \tag{37}$$

based on lagged tyre forces, where each of the eight elements are lagged to simulate relaxation within the tyre

$$\dot{\mathbf{F}}^*_{tx/y,i} = \tau^{-1}(\mathbf{F}_{tx/y,i} - \mathbf{F}^*_{tx/y,i}) \tag{38}$$

where the tyre forces $(\mathbf{F}_{txi}, \mathbf{F}_{tyi})$ are modelled according to the Pacejka magic formula

$$P(\alpha) = P(\alpha; B, C, D, E) \equiv D \sin (C \tan^{-1}(B\alpha - E(B\alpha - \tan^{-1} B\alpha))) \tag{39}$$

using normalized slip and isotropic similarity scaling (see references [**8**] and [**11**]). In more detail, the normalized slip vector is defined

$$\boldsymbol{k} = \begin{pmatrix} k_x \\ k_y \end{pmatrix} = \frac{C_\alpha}{\mathbf{F}_p} \begin{pmatrix} s \\ \tan\alpha \end{pmatrix} \tag{40}$$

where s is the longitudinal slip ratio, and α is the slip angle; these are calculated for each tyre from steer angle δ and velocities v, u, r, and ω (see for example reference [**7**]). The friction circle at each tyre contact patch is defined by the following simple analytic function of vertical load w

$$\sqrt{\mathbf{F}^2_{tx} + \mathbf{F}^2_{ty}} \leqslant \mathbf{F}_p(w) = \frac{w}{1 + (3w/2\,Mg)^3} \tag{41}$$

and the load-dependent cornering/longitudinal stiffness for each tyre is of the form

$$C_\alpha(w) = c_1\left(1 - e^{-w/c_2}\right) \tag{42}$$

(see Table 1 for values) and the resulting tyre force vector is

$$\begin{pmatrix} \mathbf{F}_{tx} \\ \mathbf{F}_{ty} \end{pmatrix} = P(|\boldsymbol{k}|)\frac{\mathbf{F}_p}{|\boldsymbol{k}|}\begin{pmatrix} k_x \\ k_y \end{pmatrix} \tag{43}$$

Vertical tyre loads are calculated from static weight distribution, and modified to accommodate lateral load transfer according to

$$\Delta_{\text{lat}} w_{\text{f/r}} = \frac{\sum \mathbf{F}_{\text{yf/r}} h_{\text{f/r}} + K_{\text{f/r}}\phi + B_{\text{f/r}} p + Mgh \sin\phi}{t_{\text{f/r}}} \tag{44}$$

and to accommodate longitudinal load transfer, approximated as

$$\Delta_{\text{long}} w = \frac{\sum_i \mathbf{F}_{xi} \cdot (h_0 + h)}{(a + b)} \tag{45}$$

with $\Delta_{\text{lat}} w_{\text{f/r}}$ and $\Delta_{\text{long}} w$ added or subtracted from the static load on each tyre in an obvious way.

This tyre model is only broadly representative of real tyre behaviour, but is thought to incorporate sufficiently realistic aspects of force saturation and load dependence to properly test the IEKF identification process. Wheel rotational dynamics are modelled as

$$\dot{\omega}_i = I_{\text{w}}^{-1}(T_i - r_r \mathbf{F}_{txi}) \tag{46}$$

where T_i is the drive torque (positive) or brake torque (negative) torque, and $I_{\text{w}} = 5$ kg m^2 is the nominal wheel inertia, incorporating tyre, engine, and driveline components. The drive torques T_i are directly commanded and apportioned equally between left and right wheels, and in the case of brake torque, apportioned in the ratio 60:40 between front and rear axles. Drive torque is apportioned entirely to the rear (RWD).